Electronic structure of intertwined kagome, honeycomb, and triangular sublattices of the intermetallics $M\mathrm{Co_2Al_9}$ (M = Sr, Ba)

Chiara Bigi,[1,2,*] Sahar Pakdel,[3] Michał J. Winiarski,[4] Pasquale Orgiani,[5] Ivana Vobornik,[5] Jun Fujii,[5] Giorgio Rossi,[5,6] Vincent Polewczyk,[5] Phil D. C. King,[1] Giancarlo Panaccione,[5] Tomasz Klimczuk,[4] Kristian Sommer Thygesen,[3,†] and Federico Mazzola[7,5,‡]

[1]*SUPA, School of Physics and Astronomy, University of St Andrews, St Andrews KY16 9SS, United Kingdom*
[2]*Synchrotron SOLEIL, F-91190 Saint-Aubin, France*
[3]*CAMD, Department of Physics, Technical University of Denmark, DK-2800 Kongens Lyngby, Denmark*
[4]*Faculty of Applied Physics and Mathematics, Advanced Materials Centre, Gdansk University of Technology, Narutowicza 11/12, PL-80-233 Gdansk, Poland*
[5]*Istituto Officina dei Materiali (IOM)-CNR, Laboratorio TASC, Area Science Park, S.S.14, Km 163.5, I-34149 Trieste, Italy*
[6]*Department of Physics, University of Milano, I-20133 Milano, Italy*
[7]*Department of Molecular Sciences and Nanosystems, Ca' Foscari University of Venice, I-30172 Venice, Italy*

(Received 24 January 2023; revised 28 May 2023; accepted 21 July 2023; published 21 August 2023)

Intermetallics are an important playground to stabilize a large variety of physical phenomena, arising from their complex crystal structure. The ease of their chemical tunabilty makes them suitable platforms to realize targeted electronic properties starting from the symmetries hidden in their unit cell. Here, we investigate the family of the recently discovered intermetallics $M\mathrm{Co_2Al_9}$ (M = Sr, Ba) and we unveil their electronic structure. By using angle-resolved photoelectron spectroscopy and density functional theory calculations, we discover the existence of Dirac-like dispersions as ubiquitous features in this family, coming from the hidden kagome and honeycomb symmetries embedded in the unit cell. Finally, from calculations, we expect that the spin-orbit coupling is responsible for opening energy gaps in the electronic structure spectrum, which also affects the majority of the observed Dirac-like states. Our study constitutes an experimental observation of the electronic structure of $M\mathrm{Co_2Al_9}$ and proposes these systems as hosts of Dirac-like physics with intrinsic spin-orbit coupling. The latter effect suggests $M\mathrm{Co_2Al_9}$ as a future platform for investigating the emergence of nontrivial topology.

DOI: 10.1103/PhysRevB.108.075148

I. INTRODUCTION

An intermetallic is a conducting alloy comprising two or more distinct metals, the crystal structure of which differs from that of the constituents. They have attracted considerable interest because of their ability to feature magnetic orders [1–3], superconducting [4–6], and half-metal behavior [7,8]. Their magnetic and electronic properties are generally attributed to a mixture of metallic, covalent, and ionic atomic bonding. Moreover, their structural complexity makes them a tantalizing platform for chemical substitution, providing the opportunity to tune their properties, often resulting in isostructural series with markedly different electronic and magnetic behavior. One notable example is given by the Heusler alloys [9,10], for which several magnetic orders have been demonstrated [11–13], putting them at the top of the list for possible candidates in spintronics applications [14–16].

$M\mathrm{Co_2Al_9}$ (M = Ba, Sr) is a new class of intermetallics, isostructural to the sister compound $\mathrm{BaFe_2Al_9}$, which exhibits a so-called "catastrophic" charge density wave transition at 100 K, with a subsequent shattering of the crystal [17]. $\mathrm{BaFe_2Al_9}$ has also been predicted to host a rich electronic structure (both above and below the charge density wave transition) with Dirac-like dispersions and flat bands, somewhat reminiscent of the electronic structure of kagome and honeycomb systems [18–21] (see Fig. 1 as an example of how these features can arise from the crystal structure). Motivated by this observation, here, we study the electronic properties of the intermetallic family $M\mathrm{Co_2Al_9}$, and we demonstrate the existence of Dirac-like bands, some of which are separated by an energy gap due to the spin-orbit coupling (SOC). With this work, we shed light on the electronic properties of $M\mathrm{Co_2Al_9}$, relating these to hidden structural metrics in the systems' unit cell, and we ultimately propose these systems as possible hosts of SOC-derived nontrivial topological properties [23–26].

Single crystals of $M\mathrm{Co_2Al_9}$, with M being Sr and Ba, were grown by using the self-flux method described in Refs. [27–29]. A powder x-ray diffraction analysis showed that both compounds crystallize into a hexagonal crystal structure belonging to the $P6/mmm$ space group [30]. Contrary to $\mathrm{BaFe_2Al_9}$ [17], both $\mathrm{SrCo_2Al_9}$ (SCA) and $\mathrm{BaCo_2Al_9}$ (BCA) do not show any phase transition down to 1.8 K [27]. The

*chiara.bigi@synchrotron-soleil.fr
†thygesen@fysik.dtu.dk
‡federico.mazzola@unive.it

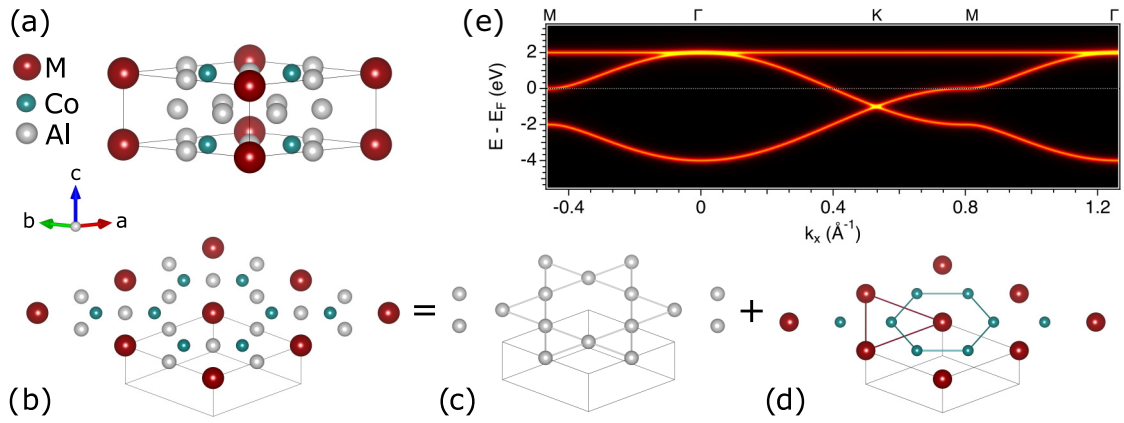

FIG. 1. MCo$_2$Al$_9$ crystal structure [22]: (a) Side view and (b) top view showing the atomic arrangement within a single unit cell. The atoms arrange themselves in a complex planar geometry which could be thought as the combination of (c) Al kagome, (d) Co honeycomb, and M triangular planes. (e) Example of an electronic structure expected for a kagome symmetry obtained by single-orbital first-neighbor tight-binding calculations. Due to this particular metric, one can expect the electronic structure to exhibit Dirac-like dispersions and flat bands.

crystals were preoriented *ex situ* along high-symmetry directions and then cleaved perpendicularly to the c axis in ultrahigh vacuum (UHV) at a base pressure of 5×10^{-11} mbar and at 77 K temperature, which was kept constant throughout the data acquisition. The metallic bonds of these systems result in a very high hardness, which makes the samples very difficult to break along the c axis. Nevertheless, we were able to apply sufficient strength to the sample to cleave it in the aforementioned conditions. We noticed that both samples showed a similar and significant quality degradation time of about 12 h, thus the angle-resolved photoelectron spectroscopy (ARPES) measurements were performed within that time range. Such a fast degradation time is consistent with a high chemical reactivity of materials containing alkali-earth metals, such as both BaCo$_2$Al$_9$ and SrCo$_2$Al$_9$. After the cleavage, all samples showed a uniform surface, with no spectroscopic variation at several positions of the beam spot (50×100 μm^2). This was also checked for multiple crystals, always yielding the same result, thus with no evidence for a termination-dependent electronic structure and no change in the spectral weight across the surface.

II. RESULTS AND DISCUSSION

The ARPES measurements were performed with different photon energies, and the electronic structure exhibits strongly varying matrix elements as well as strong changes over the photon energy range we used (40–80 eV; see Supplemental Figs. S1 and S2 [31]). The latter indicates the strong three-dimensional character of the electronic structure observed, which is also revealed by density functional theory (DFT) calculations [32–35] along the out-of-plane direction (see Supplemental Figs. S3 and S4 [31]). Such a dispersion results in a broadening of the electronic structure which is intrinsic to the system and is generally referred to as k_z broadening. The spectral intensity was prominent at 70 eV, thus we used this to better visualize the electronic structure of the MCo$_2$Al$_9$ compounds. The Fermi surfaces of MCo$_2$Al$_9$ are shown in Fig. 2 and display a nearly circular holelike pocket which occupies a large portion of the Brillouin zone (BZ). We estimated a surface-projected carrier density of $\sim0.77e^-$/cell [see methods and Fig. S1(a) [31]]. Interestingly, the matrix elements create a destructive interference which suppresses almost entirely the ARPES intensity within the first BZ. This can be observed, for example, in Fig. 2(a), where the Fermi surface of SrCo$_2$Al$_9$, centered in $(k_x, k_y) = (0, 0)$, has no intensity. Interference patterns such as the one measured for these compounds are generally a consequence of the matching between the initial and final states during the photoemission process as well as the specific experimental geometry [which we report in Fig. S1(c) [31]]. For details on these matrix element effects, see Refs. [36–40]. At first glance, the Fermi surfaces of SrCo$_2$Al$_9$ [Fig. 2(b)] and BaCo$_2$Al$_9$ [Fig. 2(d)] appear very similar in shape and size. However, BaCo$_2$Al$_9$ exhibits additional spectral features located at the BZ center [Fig. 2(d)]. Such an intensity, which is instead not detected in the Fermi surface of SrCo$_2$Al$_9$ [Fig. 2(b)], can be attributed to the presence of a more p-doped holelike band in the Ba-based compound, the intensity of which, likely helped by the large broadening of the electronic structure, spills up to the Fermi level. This can be also seen in the DFT [Figs. 2(c) and 2(e)] and highlights one of the most prized properties of isostructural intermetallics: the opportunity of sharing general common features in their electronic, thermal, and mechanical properties, but at the same time tuning such properties through chemical substitution [41–43].

To better understand the origin of the observed spectral weight, we measured the energy-momentum spectra by ARPES for both compounds and we compared them to the DFT calculations [44–46]. Overall, the DFT calculations [orange lines in Figs. 2(c) and 2(e)] track the experimental bands satisfactorily. Such bands appear broad and this is probably due to the strong chemical bonds between the atoms, which in the out-of-plane direction can give rise to an extended k_z broadening [27]. A strong three-dimensional electronic structure broadening, which is also common to other intermetallics [47], might certainly contribute to such large experimental linewidths. Plus, the three-dimensional character of these systems is also demonstrated by the strong variation along the k_z direction obtained from DFT (see

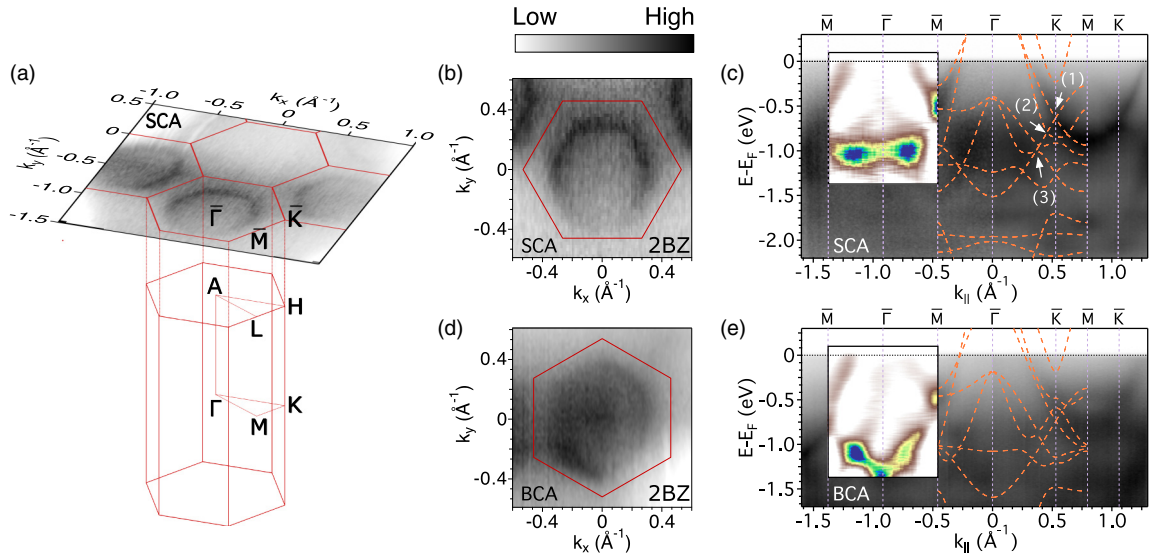

FIG. 2. (a) BZ and projected surface component along with the Fermi surface of $SrCo_2Al_9$ collected at 70 eV and with linear horizontal polarization. Strong matrix element effects hinder the detection of any photoemitted signal from the first BZ, therefore we carried out the ARPES characterization in the second zone. (b) Second BZ collected for $SrCo_2Al_9$ and (c) energy-momentum spectra along the high-symmetry directions indicated. Dashed orange lines superimposed to the ARPES data are the DFT calculated bands (with SOC). Labeled arrows mark the position of the Dirac crossings discussed in the text. (d) Second BZ collected for $BaCo_2Al_9$ and (e) energy-momentum spectra and DFT-calculated band dispersions (with SOC, dashed lines) along the high-symmetry directions indicated. Insets in (c) and (e) report the two-dimensional curvature to show the additional spectral weight close to the Fermi level for $BaCo_2Al_9$.

along Γ-*A* in Figs. S3 and S4 [31]). To help the data visualization, we plotted the curvature [48] signals along the *M*-Γ-*M* direction [see insets in Figs. 2(c) and 2(e)]. These plots readily reveal the existence of the extra intensity observed in $BaCo_2Al_9$ and centered in Γ. By comparing the data with the DFT calculations, we ascribe such a feature to the holelike bands dispersing with a maximum at Γ. Notably, the top is closer to the Fermi level for the Ba-derived compound than the Sr one, consistent with the additional spectral intensity observed in the $BaCo_2Al_9$ Fermi surface with respect to $SrCo_2Al_9$ [Figs. 2(c) and 2(e)]. The observed energy shift is large and estimated to be ∼250 meV. We stress that despite the observed holelike band being located below the Fermi level, the large tails of spectral intensity extend up to it, thus being still observable in the Fermi surface of Fig. 2(d).

To better capture the details of the electronic structure of both MCo_2Al_9, we show the DFT (without SOC) along with the calculated projected electron density of states (*p*-DOS; see Fig. 3). First, we notice that in both compounds, the main orbital character projected on the eigenstates is provided by the Al and the Co atoms, while the *M* metals seem to only contribute (in a less prominent way) to the electronic structure far away from the Fermi level (energies larger than −2 eV). The *M* metals, despite being responsible for energetic shifts, as discussed above, do not appear to contribute significantly to the near-Fermi electronic structure and fermiology. In the *p*-DOS [see Figs. 3(a) and 3(b)], several peaks with Co *d*-orbital character contribute to the main signal at a binding energy smaller than −1 eV and such peaks originate from nearly dispersionless bands. Such Co-derived localized states are not primarily linked to the flat band arising from the Al kagome motif, but rather to the strong correlations experienced by electrons in the *d* shell. Incidentally, we note that the sharp and intense peaks at $E_B \sim -1.1$ eV and at $E_B \sim -1.35$ eV in the Co *d p*-DOS are due to highly localized Co *d* bands which lie at the edge of the Brillouin zone in the *A*-*L*-*H* plane (see Figs. S3 and S4 where whole orbital-projected bulk bands are provided [31]) rather than to the kagome's flat band highlighted in red in Fig. 3(a) ("fb"). The latter possesses indeed a mainly Al *p*-orbital character, with a marginal contribution from Co, as shown in Fig. 3(c). The presence of flat bands in these materials is somewhat different from what was reported for kagome metals. In the latter, in fact, they arise from a phase-cancellation process: In a kagome, the eigenstates of the flat band have opposite sign at different sublattices, as discussed in Refs. [18,49–51]. Therefore, any electron hopping outside the hexagonal part of the kagome lattice is canceled out by a quantum destructive interference. This cancellation gives rise (within a first-neighbor tight-binding model; see Fig. 1) to a perfect localization of electrons within the BZ. In a pure kagome, both the effects of hybridization with the next-neighboring atoms and SOC can gap these states. However, their major contribution will still be given by the geometrical kagome pattern. Here, for our systems, while the Al atomic arrangement is reminiscent of a kagome lattice, there is a similar orbital contribution to such states given by the Co atoms, which develop with a honeycomb motif. The strong hybridization and overlap between the Al and Co is expected to enable bands with a dispersion significantly different from the expected textbook behavior of a pure kagome mesh. However, our calculations indicate that the flat bands [highlighted with red color in Fig. 3(a) with energy ~ -1.2 eV and in Fig. 3(b) with energy ~ -1 eV for $SrCo_2Al_9$ and $BaCo_2Al_9$, respectively] are a genuine effect of the Al atomic arrangement, since they are primarily Al derived [Fig. 3(c)]. Evidence for

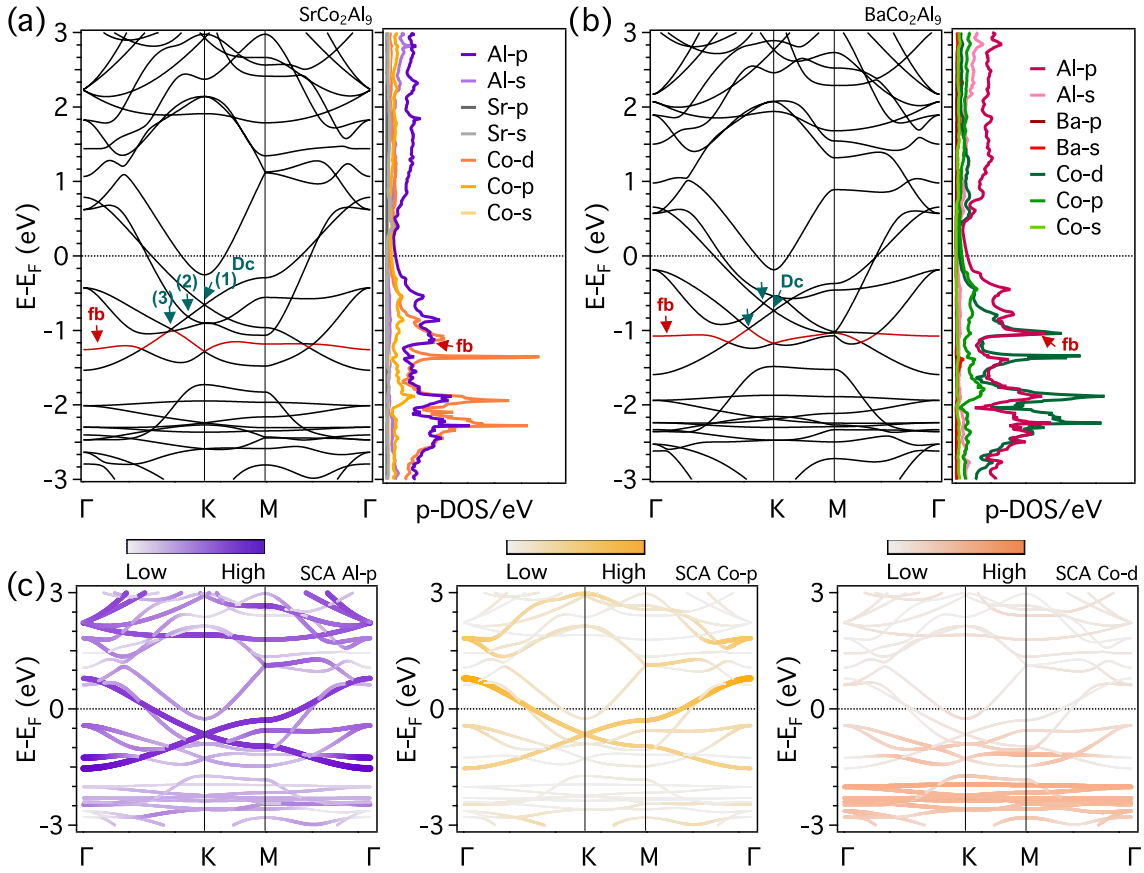

FIG. 3. *Ab initio* bulk electronic band dispersion extracted along high-symmetry directions in the Γ-*K*-*M*-Γ plane and orbital-projected partial DOS for (a) $SrCo_2Al_9$ and (b) $BaCo_2Al_9$. Labeled arrows (1)–(3) pin the Dirac-like crossings ("Dc") while the flat band ("fb") linked to the hidden Al kagome lattice is highlighted in red and marked by the red arrows both in the band dispersion and in the *p*-DOS. (c) Orbital character of the $SrCo_2Al_9$ band structure along the same high-symmetry path shows that Al *p*, Co *p*, and Co *d* orbitals bring the highest contribution to the states near E_F.

such flat states is also visible in the ARPES spectra of Fig. 2, however, they are better highlighted when linear vertical (LV) polarization was used as this suppressed the intensity from the highly dispersive bands (see Fig. S2 in where we report such spectra together with their curvature [31]).

The intrinsic honeycomb and kagome motifs created by the Co and Al respectively in both compounds is evident from a pronounced Dirac-like dispersion with a crossing point at *K*. Such a feature is clearly visible both in the experiment and in the DFT calculations, e.g., see arrow (1) in Figs. 2(c) and 3(a) ($E_B \sim -0.6$ eV) and also Fig. 3(c), indicating the hidden symmetries nestled in the crystal structure of both intermetallics. This band crossing is present for both compounds and has a van Hove singularity at the *M* point approximately 300 meV (400 meV) below the Fermi level for $SrCo_2Al_9$ ($BaCo_2Al_9$). Due to strong matrix element effects its presence in Fig. 2 is concealed by the intense highly dispersive states along *K*-*M* (for better visualization, see Fig. S5 where we probe the van Hove singularity in different geometries to better highlight it [31]). According to our orbital-projected DFT, similarly to graphene, such a Dirac dispersion appears to derive from *p*-type orbitals, in this case with mixed Al-Co character. We notice also that the same bands which develop into a Dirac-like dispersion are the same that in the experiment give rise to the largest circular Fermi surface as in Fig. 2. We notice that such bands, in proximity of the Fermi level, are very close to each other, thus giving rise, within our resolution, to a single ring rather than the two that are theoretically expected. If, on the one hand, the MCo_2Al_9 bears several similarities with graphene, we notice remarkable differences: In graphene, the energy difference between the Dirac crossing and the van Hove singularity is large, i.e., approximately 3 eV [52,53]. Here, it is instead one order of magnitude smaller, i.e., approximately 0.3 eV. This strikingly different behavior could be exploited by filling or depopulating the singularity point owing to the ease of tunability offered by this family of materials. Once these states are brought to the Fermi level, they could lead to a collective phase transition. A notable example is $BaFe_2Al_9$ where the Al-derived van Hove singularity and Dirac cones cross the Fermi level and $BaFe_2Al_9$ undergoes a charge density wave transition so strong that the crystal shatters [17]. Finally, the lower branch of the Dirac cone intersects other highly dispersive bands along Γ-*K*; see, for example, $E_B \sim -0.8$ eV [green arrow (2)] and $E_B \sim -1$ eV [green arrow (3)] in Fig. 3(a). These crossing bands are also characterized by a strong intermixing of Al-Co orbitals, with the only difference being that this time the Co *d* orbitals hybridize with the Al *p* character.

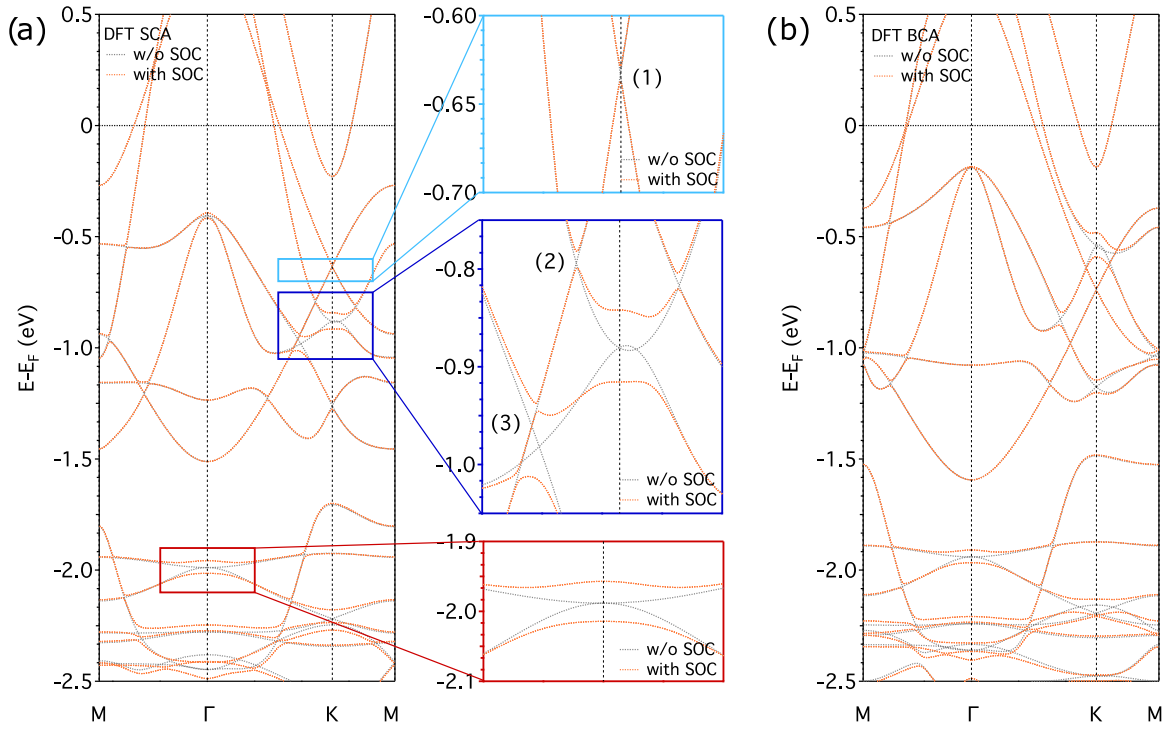

FIG. 4. Effects of SOC on the electronic band structure of (a) $SrCo_2Al_9$ and (b) $BaCo_2Al_9$. Zoom-in of the colored boxes in (a) shows details of the anticrossing opening gaps induced by SOC at the K and Γ points. Labels (1)–(3) mark the positions of the Dirac crossings discussed above.

SOC further mixes the orbital character of the bands, introducing energy gaps in the MCo_2Al_9 band structure (see Fig. 4 for bands with and without SOC, orange and gray, respectively). According to the DFT, the effect of the SOC is stronger in the bands displaying a Co d character and manifests by gapping Dirac-like states at both the K and Γ points. Specifically, $SrCo_2Al_9$ displays such energy gaps of ∼70 meV at the K point (blue framed zoom) and of ∼60 meV at Γ (red frame). In the kagome metals such as the recently discovered XV_6Sn_6 family (X = Gd, Y, Tb) [54–56], spin-orbit-induced gaps in the electronic structure have attracted attention because they are expected to host a finite contribution to the spin Berry curvature. This has been recently proved by Di Sante *et al.* in Ref. [57] and it applies also to other systems as that partially discussed in Ref. [58] for $TaCoTe_2$. Our system, which intrinsically hosts this lattice, is not expected to behave differently (and with the additional ease of intermetallics to tune such properties even further by chemical substitution), thus our work invites further study of this topological aspect.

III. CONCLUSIONS

Summarizing, the combination of ARPES and DFT allows us to discover the presence of several Dirac-like dispersions in the MCo_2Al_9 intermetallic family, hidden in the honeycomb/kagome substructures. Orbital-projected DFT consistently pinpoints a strong Al-Co hybridization across the whole Dirac-like band structure. Finally, our DFT reveals the existence of sizable SOC-induced gaps in most of the crossings. We therefore establish the benchmarks of the electronic properties of these compounds and pave the way for further studies of SOC-derived phenomena and the development of nontrivial topology in the series.

The research data supporting this publication can be accessed at Ref. [59].

ACKNOWLEDGMENTS

This work has been performed in the framework of the Nanoscience Foundry and Fine Analysis (NFFA-MIUR Italy Progetti Internazionali) facility. C.B. and P.D.C.K. gratefully acknowledge support from The Leverhulme Trust via Grant No. RL-2016-006. F.M. greatly acknowledges the SoE action of pnrr, No. SOE_0000068. K.S.T. and S.P. acknowledge funding from the European Research Council (ERC) under the European Union's Horizon 2020 research and innovation program Grant No. 773122 (LIMA). K.S.T. is a Villum Investigator supported by VILLUM FONDEN (Grant No. 37789).

F.M., C.B., J.F., G.P., G.R., I.V., P.K., V.P., and P.O. performed the ARPES measurements and C.B. and F.M. analyzed the data. S.P. and K.T. performed the theoretical calculations and M.W. and T.K. performed the growth and characterization of the samples. All authors contributed in writing the manuscript. F.M. conceived and led the project.

The authors confirm that there are no competing financial interests.

[1] Y. Zhang, J. Alloys Compd. **787**, 1173 (2019).
[2] K. Kamishima, T. Goto, H. Nakagawa, N. Miura, M. Ohashi, N. Mori, T. Sasaki, and T. Kanomata, Phys. Rev. B **63**, 024426 (2000).
[3] F. Kabir, R. Filippone, G. Dhakal, Y. Lee, N. Poudel, J. Casey, A. P. Sakhya, S. Regmi, R. Smith, P. Manfrinetti *et al.*, Phys. Rev. Mater. **6**, 064404 (2022).
[4] R. Cava, H. Takagi, H. Zandbergen, J. Krajewski, W. Peck, T. Siegrist, B. Batlogg, R. Van Dover, R. Felder, K. Mizuhashi *et al.*, Nature (London) **367**, 252 (1994).
[5] T. Klimczuk, C. H. Wang, K. Gofryk, F. Ronning, J. Winterlik, G. H. Fecher, J.-C. Griveau, E. Colineau, C. Felser, J. D. Thompson, D. J. Safarik, and R. J. Cava, Phys. Rev. B **85**, 174505 (2012).
[6] H. Su, F. Du, R. Li, S. Luo, Y. Chen, J. Liu, Y. Chen, C. Cao, M. Smidman, and H. Yuan, Phys. Rev. B **106**, 134517 (2022).
[7] T. Kono, M. Kakoki, T. Yoshikawa, X. Wang, K. Goto, T. Muro, R. Y. Umetsu, and A. Kimura, Phys. Rev. Lett. **125**, 216403 (2020).
[8] Q. Gao, Z. Li, M. Ma, J. Tu, R. Wang, Q. Liu, Z. Chen, Y. Zhang, Y. Sun, J. Ning *et al.*, AIP Adv. **12**, 025005 (2022).
[9] F. Heusler and E. Take, Trans. Faraday Soc. **8**, 169 (1912).
[10] K. Manna, Y. Sun, L. Muechler, J. Kübler, and C. Felser, Nat. Rev. Mater. **3**, 244 (2018).
[11] I. Belopolski, K. Manna, D. S. Sanchez, G. Chang, B. Ernst, J. Yin, S. S. Zhang, T. Cochran, N. Shumiya, H. Zheng *et al.*, Science **365**, 1278 (2019).
[12] J. Finley, C.-H. Lee, P. Y. Huang, and L. Liu, Adv. Mater. **31**, 1805361 (2019).
[13] M. Halder, S. M. Yusuf, A. Kumar, A. K. Nigam, and L. Keller, Phys. Rev. B **84**, 094435 (2011).
[14] Y. He, G. H. Fecher, C. Fu, Y. Pan, K. Manna, J. Kroder, A. Jha, X. Wang, Z. Hu, S. Agrestini *et al.*, Adv. Mater. **32**, 2004331 (2020).
[15] C. Guillemard, S. Petit-Watelot, L. Pasquier, D. Pierre, J. Ghanbaja, J. C. Rojas-Sánchez, A. Bataille, J. Rault, P. Le Fèvre, F. Bertran, and S. Andrieu, Phys. Rev. Appl. **11**, 064009 (2019).
[16] Y. P. Kabanov, R. D. Shull, C. Zheng, P. W. Pong, and D. B. Gopman, Appl. Surf. Sci. **536**, 147672 (2021).
[17] W. R. Meier, B. C. Chakoumakos, S. Okamoto, M. A. McGuire, R. P. Hermann, G. D. Samolyuk, S. Gao, Q. Zhang, M. B. Stone, A. D. Christianson *et al.*, Chem. Mater. **33**, 2855 (2021).
[18] M. Kang, S. Fang, L. Ye, H. C. Po, J. Denlinger, C. Jozwiak, A. Bostwick, E. Rotenberg, E. Kaxiras, J. G. Checkelsky *et al.*, Nat. Commun. **11**, 4004 (2020).
[19] S. Okamoto, N. Mohanta, E. Dagotto, and D. N. Sheng, Commun. Phys. **5**, 198 (2022).
[20] M. Han, H. Inoue, S. Fang, C. John, L. Ye, M. K. Chan, D. Graf, T. Suzuki, M. P. Ghimire, W. J. Cho *et al.*, Nat. Commun. **12**, 5345 (2021).
[21] M. Polini, F. Guinea, M. Lewenstein, H. C. Manoharan, and V. Pellegrini, Nat. Nanotechnol. **8**, 625 (2013).
[22] K. Persson, Materials data on $SrAl_9Co_2$ (SG:191) by Materials Project (LBNL, CA, USA, 2014), doi:10.17188/1191902.
[23] J. Zhang, B. Zhao, T. Zhou, Y. Xue, Y. Fang, C. Ma, and Z. Yang, Phys. Rev. B **99**, 035409 (2019).
[24] K. Choudhary, K. F. Garrity, and F. Tavazza, Sci. Rep. **9**, 8534 (2019).
[25] J.-X. Yin, S. S. Zhang, G. Chang, Q. Wang, S. S. Tsirkin, Z. Guguchia, B. Lian, H. Zhou, K. Jiang, I. Belopolski *et al.*, Nat. Phys. **15**, 443 (2019).
[26] W. Zhang and W. Yi, Nat. Commun. **4**, 2711 (2013).
[27] Z. Ryżyńska, T. Klimczuk, and M. J. Winiarski, J. Solid State Chem. **289**, 121509 (2020).
[28] P. C. Canfield and Z. Fisk, Philos. Mag. B **65**, 1117 (1992).
[29] P. C. Canfield, T. Kong, U. S. Kaluarachchi, and N. H. Jo, Philos. Mag. **96**, 84 (2016).
[30] K. Turban and H. Schäfer, J. Less-Common Met. **40**, 91 (1975).
[31] See Supplemental Material at http://link.aps.org/supplemental/10.1103/PhysRevB.108.075148 for additional ARPES data and the full set of orbital-projected bulk band structures as obtained from DFT, as well as technical details regarding sample preparation, ARPES measurements, and theoretical calculations useful to understand the results shown in the main text.
[32] W. Kohn and L. J. Sham, Phys. Rev. **140**, A1133 (1965).
[33] P. E. Blöchl, Phys. Rev. B **50**, 17953 (1994).
[34] J. Enkovaara, C. Rostgaard, J. J. Mortensen, J. Chen, M. Dułak, L. Ferrighi, J. Gavnholt, C. Glinsvad, V. Haikola, H. A. Hansen *et al.*, J. Phys.: Condens. Matter **22**, 253202 (2010).
[35] J. J. Mortensen, L. B. Hansen, and K. W. Jacobsen, Phys. Rev. B **71**, 035109 (2005).
[36] F. Boschini, D. Bugini, M. Zonno, M. Michiardi, R. P. Day, E. Razzoli, B. Zwartsenberg, M. Schneider, E. H. da Silva Neto, S. dal Conte *et al.*, New J. Phys. **22**, 023031 (2020).
[37] F. Mazzola, J. W. Wells, R. Yakimova, S. Ulstrup, J. A. Miwa, R. Balog, M. Bianchi, M. Leandersson, J. Adell, P. Hofmann *et al.*, Phys. Rev. Lett. **111**, 216806 (2013).
[38] F. Mazzola, T. Frederiksen, T. Balasubramanian, P. Hofmann, B. Hellsing, and J. W. Wells, Phys. Rev. B **95**, 075430 (2017).
[39] M. Mulazzi, G. Rossi, J. Braun, J. Minár, H. Ebert, G. Panaccione, I. Vobornik, and J. Fujii, Phys. Rev. B **79**, 165421 (2009).
[40] R. P. Day, B. Zwartsenberg, I. S. Elfimov, and A. Damascelli, npj Quantum Mater. **4**, 54 (2019).
[41] A. Continenza and P. Monachesi, J. Magn. Magn. Mater. **104-107**, 1308 (1992).
[42] R. Meng, B. Lorenz, J. Cmaidalka, Y. Wang, Y. Sun, J. Lenzi, J. Meen, Y. Xue, and C. Chu, IEEE Trans. Appl. Supercond. **13**, 3042 (2003).
[43] A. Continenza and P. Monachesi, Phys. Rev. B **46**, 6217 (1992).
[44] M. Gjerding, T. Skovhus, A. Rasmussen, F. Bertoldo, A. H. Larsen, J. J. Mortensen, and K. S. Thygesen, Comput. Mater. Sci. **199**, 110731 (2021).
[45] A. H. Larsen, J. J. Mortensen, J. Blomqvist, I. E. Castelli, R. Christensen, M. Dułak, J. Friis, M. N. Groves, B. Hammer, C. Hargus *et al.*, J. Phys.: Condens. Matter **29**, 273002 (2017).
[46] J. P. Perdew, K. Burke, and M. Ernzerhof, Phys. Rev. Lett. **77**, 3865 (1996).
[47] Q. Y. Chen, C. H. P. Wen, Q. Yao, K. Huang, Z. F. Ding, L. Shu, X. H. Niu, Y. Zhang, X. C. Lai, Y. B. Huang *et al.*, Phys. Rev. B **97**, 075149 (2018).
[48] P. Zhang, P. Richard, T. Qian, Y.-M. Xu, X. Dai, and H. Ding, Rev. Sci. Instrum. **82**, 043712 (2011).
[49] M. Li, Q. Wang, G. Wang, Z. Yuan, W. Song, R. Lou, Z. Liu, Y. Huang, Z. Liu, H. Lei *et al.*, Nat. Commun. **12**, 3129 (2021).

[50] Z. Li, J. Zhuang, L. Wang, H. Feng, Q. Gao, X. Xu, W. Hao, X. Wang, C. Zhang, K. Wu *et al.*, Sci. Adv. **4**, eaau4511 (2018).

[51] M. Kang, L. Ye, S. Fang, J.-S. You, A. Levitan, M. Han, J. I. Facio, C. Jozwiak, A. Bostwick, E. Rotenberg *et al.*, Nat. Mater. **19**, 163 (2020).

[52] B. Hellsing, T. Frederiksen, F. Mazzola, T. Balasubramanian, and J. W. Wells, Phys. Rev. B **98**, 205428 (2018).

[53] F. Bisti, G. Profeta, H. Vita, M. Donarelli, F. Perrozzi, P. M. Sheverdyaeva, P. Moras, K. Horn, and L. Ottaviano, Phys. Rev. B **91**, 245411 (2015).

[54] G. Pokharel, S. M. L. Teicher, B. R. Ortiz, P. M. Sarte, G. Wu, S. Peng, J. He, R. Seshadri, and S. D. Wilson, Phys. Rev. B **104**, 235139 (2021).

[55] G. Pokharel, B. Ortiz, J. Chamorro, P. Sarte, L. Kautzsch, G. Wu, J. Ruff, and S. D. Wilson, Phys. Rev. Mater. **6**, 104202 (2022).

[56] E. Rosenberg, J. M. DeStefano, Y. Guo, J. S. Oh, M. Hashimoto, D. Lu, R. J. Birgeneau, Y. Lee, L. Ke, M. Yi *et al.*, Phys. Rev. B **106**, 115139 (2022).

[57] D. Di Sante, C. Bigi, P. Eck, S. Enzner, A. Consiglio, G. Pokharel, P. Carrara, P. Orgiani, V. Polewczyk, J. Fujii *et al.*, Nat. Phys. **19**, 1135 (2023).

[58] F. Mazzola, B. Ghosh, J. Fujii, G. Acharya, D. Mondal, G. Rossi, A. Bansil, D. Farias, J. Hu, A. Agarwal *et al.*, Nano Lett. **23**, 902 (2023).

[59] C. Bigi, S. Pakdel, M. Winiarski, P. Orgiani, I. Vobornik, J. Fujii, G. Rossi, V. Polewczyk, P. King, G. Panaccione, T. Klimczuk, K. Thygesen, and F. Mazzola, The electronic structure of intertwined kagome, honeycomb, and triangular sublattices of the intermetallics MCo2Al9 (dataset), Dataset, University of St Andrews Research Portal (2023), https://doi.org/10.17630/54b8baa0-05b4-4649-a034-d3da4943bde9.